# Enhancement of harmonics for optically detected light- and heavy-hole cyclotron resonance in germanium

Tatsuya Tomaru, Tyuzi Ohyama, and Eizo Otsuka
*Department of Physics, College of General Education, Osaka University, Toyonaka, Osaka 560, Japan*
(Received 26 November 1990)

Heavy-hole cyclotron harmonic resonance to sixth order, and light-hole cyclotron harmonic resonance to third order, have been observed in high-purity Ge by means of optically detected cyclotron resonance (ODCR). It is found that hole cyclotron resonance and its harmonics are more pronounced in ODCR than in ordinary cyclotron resonance, possibly leading to a clearer description of the hot-hole distribution under resonance conditions. Hot holes produced by fundamental cyclotron resonance are distributed rather uniformly in wave-vector space; on the other hand, hot holes produced by harmonic resonances are localized in such a region that $k_3 \approx 0$, where $k_3$ is the wave-vector component parallel to the external magnetic field.

## I. INTRODUCTION

Degeneracy at the valence-band edge in cubic semiconductors, such as Si and Ge, is the origin of the characteristic behavior of holes in transport as well as optical properties of these materials; namely, cyclotron harmonic resonance,[1,2] many quantum lines of cyclotron resonance (CR),[3,4] negative effective mass,[5] and laser action using heavy- and light-hole bands.[6] In this paper we will report observations on cyclotron harmonic resonance in high-purity Ge among these topics.

Cyclotron resonance was first introduced to solid-state physics as a direct method of determining the effective masses of carriers, and subsequently developed into a tool to investigate scattering phenomena in semiconductors.[7]

With regard to harmonics, Dresselhaus, Kip, and Kittel[8] reported them as extra lines of cyclotron resonance, while Dexter, Zeiger, and Lax[1] identified them as the second and third harmonics of heavy-hole cyclotron resonance. Concerning higher-order harmonic resonance of heavy holes and that of light holes, there is only a brief report by Gverdtsiteli, Aleksandrov, and Ovchinnikova.[9] Here, we have observed harmonics of heavy holes to sixth order and those of light holes to third order not by means of ordinary cyclotron resonance but by optically detected cyclotron resonance (ODCR). Observation of such higher-order harmonics in ODCR has not been, to our knowledge, previously reported.

Optically detected cyclotron resonance was observed in Ge by Baranov *et al.*[10] Later ODCR was used on some other materials,[11–16] but the use of the technique did not make significant progress because of the poor signal-to-noise ratio. Recently, we have succeeded in observing very clear ODCR signals.[17] In that paper we discuss the mechanism as well as the advantage of ODCR.

Detailed experimental as well as theoretical studies of the valence-band edge in Ge were made by Hensel and Suzuki,[3,4] to determine accurately the five parameters in Luttinger's Hamiltonian[18,19] by means of cyclotron resonance with the help of uniaxial stress. They exactly predicted peak positions of quantum hole cyclotron resonance and explained well experimental results under thermal equilibrium. However, the hot-hole problem has not been studied enough so far. Optically detected cyclotron resonance signal directly reflects the information of hot holes, not to mention that of hot electrons, which will be discussed in Sec. IV.

In what follows, we will report pronounced harmonics in optically detected hole cyclotron resonance. We will further discuss a relation between the experimental results and the hot-hole distribution problem.

## II. EXPERIMENTAL PROCEDURE

We used a high-purity Ge sample in this experiment, where $N_A - N_D \lesssim 10^{12}$ cm$^{-3}$ and sample size of $3.5 \times 3.5 \times 1.6$ mm$^3$. After both $(\bar{1}10)$ crystallographic faces of $3.5 \times 3.5$ mm$^2$ were mechanically polished, the sample was etched by CP4A solution ($HNO_3$:HF:$CH_3COOH = 5:3:3$).

Optically detected cyclotron resonance is observed as a change in the photoluminescence spectrum caused by cyclotron resonance. In order to get ODCR signals, we monitored the LA-phonon-assisted electron-hole droplet (EHD) line[20] on the photoluminescence spectrum of the sample and took ODCR signals by sweeping external magnetic field.

The experimental setup is basically the same as that in Ref. 17. Figure 1 shows the block diagram of the measuring system. A part of the equipment related to optical fibers has been improved (see Fig. 2). Using the improved system, we have been able to observe very small changes in the photoluminescence signal due to cyclotron resonance. The sample was set in a rectangular waveguide for 35-GHz microwaves—one $(\bar{1}10)$ face of the sample was pasted on the interior of the waveguide by Apiezon grease—in such a way that the microwave electric field was always perpendicular to the $(\bar{1}10)$ plane of the sample. The sample was directly immersed in liquid helium in order to avoid the heating effect. Experiments

 

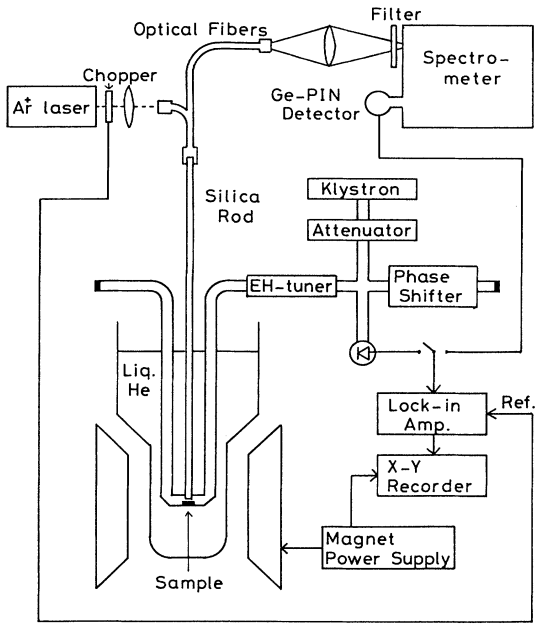


FIG. 1. Block diagram of the experimental setup.

were always carried out at temperatures between 1.5 and 4.2 K. External magnetic field by means of electromagnet was applied along any arbitrary direction in the $(\bar{1}10)$ plane of the sample and always perpendicular to the microwave electric field. This is a configuration to observe the transverse cyclotron resonance. (See Ref. 2 or Table II.)

Both photoluminescence and excitation light by means of an $Ar^+$-ion laser were guided by a silica rod (3 mm diameter) and specially designed optical silica fibers. Details of the optical fibers is schematically shown in Fig. 2. One end of the optical fibers was bundled into a form of concentric circles, with an inner diameter of 1.5 mm and an outer diameter of 3.0 mm. The other end of the bundle was formed into a rectangle of $5.3 \times 1$ mm$^2$ for the purpose of fitting to the slit of the spectrometer (JASCO CT-50). To prevent direct incidence of undesirable light to the spectrometer, a piece of suitable color glass filter was used. The detector was Ge-PIN photodiode (NORTH COAST EO-817). The signal was caught by a lock-in amplifier with a light modulation technique. The signal of ordinary cyclotron resonance absorption was also taken in the same condition as the case of the ODCR measurement.

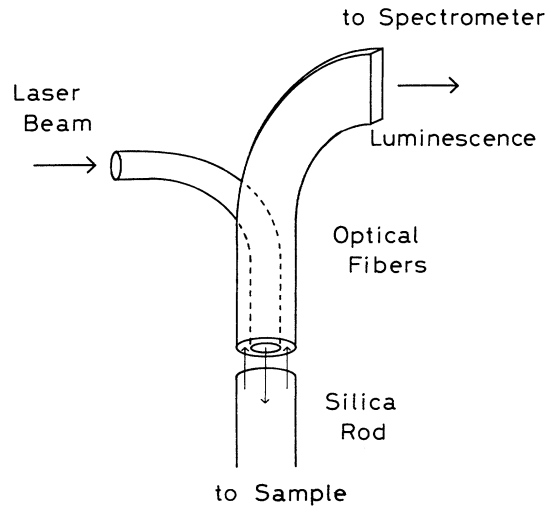


FIG. 2. Details of the part of optical fibers in Fig. 1.

## III. EXPERIMENTAL RESULTS

Figures 3(a) and 4 are ODCR signals taken with the external magnetic field being applied along 35° and 70° off

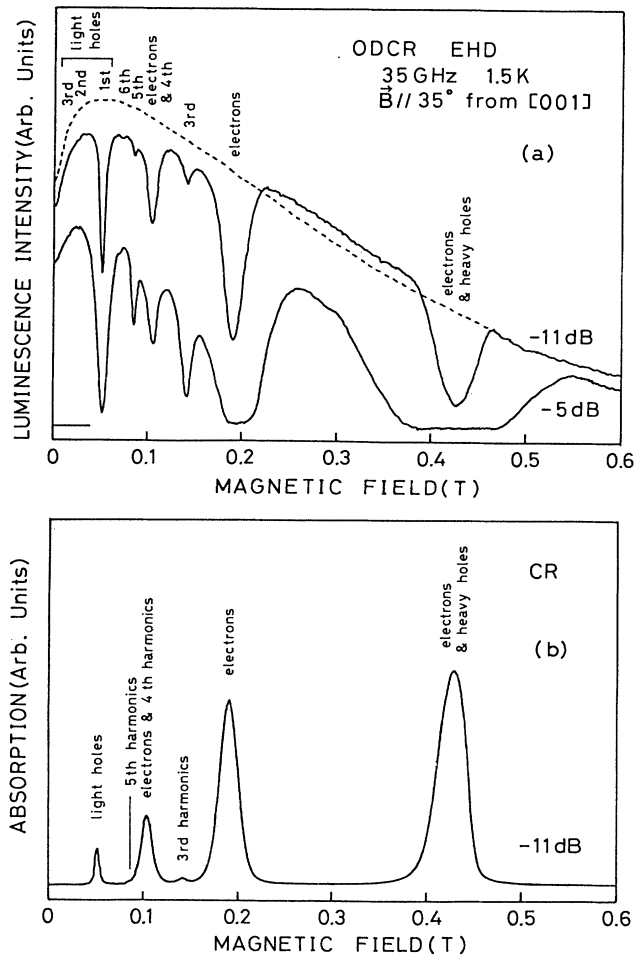


FIG. 3. (a) Typical ODCR signals obtained from EHD (LA) line (Ref. 20); relative microwave powers are expressed on the right side. The broken line exhibits magnetic-field dependence of photoluminescence intensity in the absence of incident microwaves. Dips in the solid lines show electron cyclotron resonance, light- and heavy-hole cyclotron resonances, and their harmonics; the second harmonic of heavy-hole resonance lies on the right side of electron resonance at 0.19 T, somewhat visible when the microwave power is $-5$ dB. (b) Ordinary cyclotron resonance signal under the same condition as the upper signal in (a).

the [001] crystallographic direction, respectively. Since the EHD are broken through impact of free carriers which are heated up through cyclotron resonance absorption, the intensity of the EHD line on the photoluminescence spectrum decreases at resonance positions. Dips in ODCR traces in Figs. 3(a) and 4 indicate cyclotron resonance of free carriers.

The resonance condition of harmonics as well as fundamental resonance is given by the relation $\omega = neB_c/m^*$, where $\omega$, $B_c$, $m^*$, and $n$ are the angular frequency of the microwaves, the resonance magnetic field, the effective mass of the charged particles, and an integer, respectively. The $n$th harmonic resonance is, accordingly, observed with magnetic field one $n$th as high as the fundamental resonance. In other words, harmonic resonance would occur as if charged particles had heavy- or light-hole effective mass divided by an integer. Angular dependence of the hole effective masses obtained from dip positions of ODCR signals is shown by open circles in Fig. 5. Sometimes harmonic signals, especially the second, of heavy-hole resonance are not resolved because of the overlapping by the strong electron resonance line. The top solid line shows the angular dependence of heavy-hole effective mass theoretically estimated from the expansion formula for effective mass and the band parameters given by Levinger and Frankl,[21] whose values are probably most accurate of all obtained so far through classical cyclotron resonance experiments. The solid line for the theoretical effective mass of light holes was estimated in the same

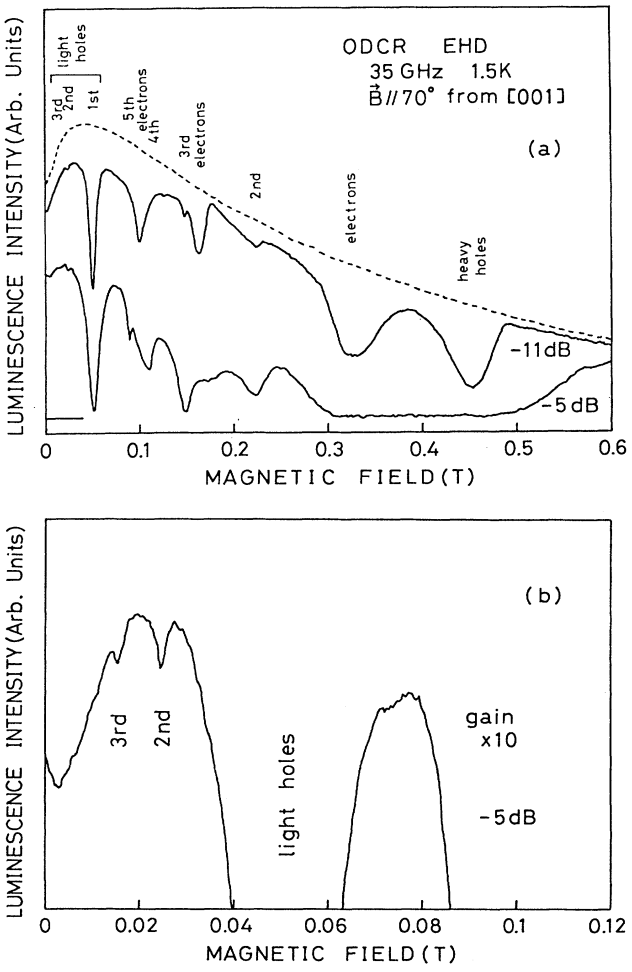


FIG. 4. (a) ODCR signals under the same condition as in Fig. 3 except for external magnetic-field direction. Three resonance lines, i.e., electron cyclotron resonance, the forth and fifth harmonics of heavy-hole resonance, overlap at ~0.1 T. Electron resonance is dominant for −11 dB microwave power, while the fourth and fifth harmonics of heavy-hole resonance are dominant for −5 dB microwave power. (b) Local magnification of (a). The second and third harmonics of light-hole cyclotron resonance are clearly observed.

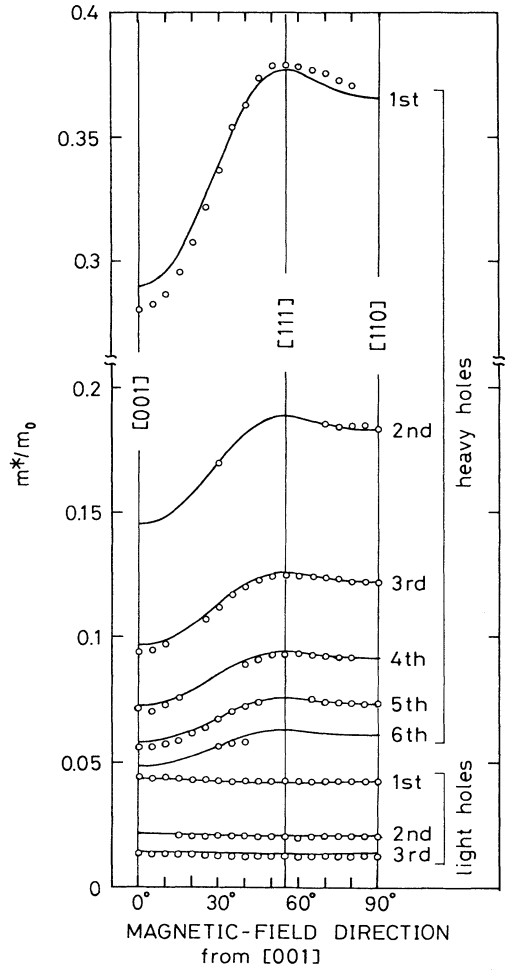


FIG. 5. The angular dependence of hole effective masses obtained from dip positions of ODCR signals, using the relation $\omega = eB_c/m^*$. See text about the solid lines. At some directions, resonance positions are hard to identify. For example, the second harmonic of heavy-hole cyclotron resonance cannot be distinguished in low-angle regions because of the overlapping by the strong electron resonance line. In the case of the magnetic-field direction being in a $(\bar{1}10)$ plane of the sample, the sixth harmonic of heavy-hole cyclotron resonance is observed only when the magnetic field is applied along 30°–40° off the [001] direction.

TABLE I. Qualitative dependence of signal intensity of cyclotron harmonic resonance on magnetic-field direction. Angles in the table show those between the magnetic-field direction and [001] direction of the sample. The magnetic field is rotated within the $(\bar{1}10)$ plane: 0° corresponds to **B**‖[001], 55° to **B**‖[111], and 90° to **B**‖[110].

| | Heavy holes |
|---|---|
| 1st | No large variation |
| 2nd | Gradual increase at 65°–90° |
| 3rd | Gradual increase at 55°–90°, but impossible to judge at 0°–55° owing to overlapping peaks |
| 4th | Relatively weak at 0°–15°, while relatively strong at 40°–80° |
| 5th | Relatively strong at 0°–45° and weak at 65°–90° |
| 6th | Observable only around 30° to 40°. |
| | **Light holes** |
| 1st | No large variation |
| 2nd | No peak at 0°–10°, and graudal increase at 15°–90° |
| 3rd | Gradual decrease at 0°–55°, and gradual increase at 55°–90° |

way. Band parameters obtained by classical cyclotron resonance (thermal energy much greater than cyclotron energy) are somewhat different from those obtained by quantum cyclotron resonance (thermal energy much less than cyclotron energy).[4] This is because the classical cyclotron resonance line is a gathering of all quantum resonance lines, and yet analysis is done as the classical limit. In dealing with the resonance of hot holes, we should use the parameters in the classical region. The other solid lines in Fig. 5 were obtained from the effective mass of heavy or light holes divided by the integer. Agreement between experimental effective masses and solid lines is fairly good as shown in Fig. 5; slight disagreement mainly arises from the uncertainty of the band parameters. Intensity of the resonances we identify as harmonics in Figs. 3(a) and 4 increases with microwave power, so that these resonances are not the quantum lines arising from transitions between low-lying Landau levels but harmonics of cyclotron resonance. The quantum cyclotron resonance is prominent only when the microwave power is low and the carrier population at lower Landau levels is large.

Figure 3(b) shows an ordinary cyclotron resonance signal under the same condition as we have obtained the ODCR signal in Fig. 3(a). We have briefly reported in Ref. 17 that the relative intensity of harmonic against fundamental resonance is larger in ODCR than in ordinary cyclotron resonance. The characteristic is just seen in Fig. 3, that is, harmonic resonances are more pronounced in ODCR than in ordinary cyclotron resonance. For example, the sixth harmonic is observable in Fig. 3(a), while not in Fig. 3(b). Because of this characteristic, we have clearly observed harmonic resonance to the third order for light holes and to the sixth order for heavy holes by means of ODCR. Harmonic resonances of light holes are shown in Fig. 4(b).

In Table I we show only the qualitative result for the angular dependence of the observed signal intensity. We also show selection rules of cyclotron harmonic resonance in Table II for reference.[3] Focusing our attention on the third harmonic of light-hole resonance, one finds that the result in Table I and selection rules in Table II are consistent with each other. The reason why the third harmonic was observable at **B**‖[111] is probably due to weak mixing of longitudinal resonance caused by disorder of microwaves in the waveguide. As for the second harmonic of light-hole resonance, on the other hand, we cannot explain the experimental result. Table I shows that the signal intensity of the second harmonic is strongest in case of **B**‖[110]. Table II, however, shows that in this case the transverse resonance is forbidden and only the longitudinal is allowed, which should be very weak in our experimental configuration. Nevertheless, we obtained a very strong signal. Such a strong longitudinal resonance cannot be explained merely by disorder of microwaves.

One may also note in Fig. 3 that the relative intensity of the hole cyclotron resonance against the electron resonance is larger in ODCR than in CR. This indicates the difference between hot-hole and hot-electron states, and the difference in EHD-dissociation efficiency between hot holes and hot electrons.[17]

TABLE II. Selection rules of cyclotron harmonic resonance at various magnetic-field directions, obtained from the theory based on Luttinger's Hamiltonian. General selection rules are given in Table IV of Ref. 3. Circles show allowed transitions, while crosses show forbidden ones. Transverse or longitudinal cyclotron resonance is the case when the microwave electric field is perpendicular or parallel to the external magnetic field, respectively (Ref. 2). The wave-vector component parallel to the magnetic field $k_3$ is an important element for the selection rules. The selection rules are common to light and heavy holes. The fifth harmonic in the case of $k_3=0$ at **B**‖[111] satisfies the selection rules about rotational symmetry and parity conservation, so that it is an allowed transition in accordance with Table IV in Ref. 3. A concrete expression (Ref. 22) of Luttinger's Hamiltonian, however, indicates that it is forbidden. We take it as forbidden.

| | Magnetic-field direction | Transverse | | Longitudinal | |
|---|---|---|---|---|---|
| | | $k_3=0$ | $k_3\neq0$ | $k_3=0$ | $k_3\neq0$ |
| 1st | [001] | ○ | ○ | × | × |
| | [111] | ○ | ○ | × | × |
| | [110] | ○ | ○ | × | × |
| 2nd | [001] | × | × | × | × |
| | [111] | × | ○ | × | × |
| | [110] | × | × | × | ○ |
| 3rd | [001] | ○ | ○ | × | × |
| | [111] | × | × | ○ | ○ |
| | [110] | ○ | ○ | × | × |
| 4th | [001] | × | × | × | ○ |
| | [111] | × | ○ | × | × |
| | [110] | × | × | × | ○ |
| 5th | [001] | ○ | ○ | × | × |
| | [111] | × | ○ | × | × |
| | [110] | ○ | ○ | × | × |
| 6th | [001] | × | × | × | × |
| | [111] | × | × | × | ○ |
| | [110] | × | × | × | ○ |

In addition, one may note that the photoluminescence intensity slightly increases for the magnetic field of 0.23–0.38 T with the influence of microwaves when the relative microwave power is −11 dB in Fig. 3(a). This is probably due to interaction between EHD and the microwaves, say for example, enhancement of the EHD formation rate induced by microwaves. Detailed discussion, however, will be given in a separate paper.

## IV. DISCUSSION

The mechanism of ODCR is as follows: Free carriers are first heated up through cyclotron resonance absorption and become hot. Next they collide against radiative objects contributing to the monitored photoluminescence, say EHD, and break radiative objects through an impact dissociation process.[17] Signals of ODCR, accordingly, offer two kinds of information to us: (1) that of hot carriers, and (2) that of an impact dissociation process on hot carriers against radiative objects. As for the latter, we have discussed in Ref. 23 that interaction between the same kind of charged particles is dominant in the impact dissociation process. In this section we treat the former and discuss the momentum distribution of hot holes under the resonance condition, by considering the warped energy surface of hole bands derived from a semiclassical treatment and by considering the transition probabilities of cyclotron resonance and its harmonics calculated from quantum theory. Here the difference between fundamental and harmonic resonances is emphasized. Finally we try to clarify the reason why harmonics are more pronounced in ODCR than in CR.

The appearance of harmonics in cyclotron resonance spectra originates in the warping of the energy surface at the valence-band top. This warped energy surface is given by

$$\varepsilon=\frac{\hbar^2}{2m_0}\{Ak^2\pm[B^2k^4+C^2(k_x^2k_y^2+k_y^2k_z^2+k_z^2k_x^2)]^{1/2}\}\ , \tag{1}$$

where $A$, $B$, and $C$ are band parameters,[8] $m_0$ the free electron mass, and $\mathbf{k}=(k_x,k_y,k_z)$ the wave vector. The subscripts $x$, $y$, and $z$ indicate the crystal principal axes. The (+) and (−) signs refer to light- and heavy-hole bands, respectively. Rewriting this equation artificially,[2] one gets

$$\varepsilon=\frac{\hbar^2k^2}{2m}(1+g)\ , \tag{2}$$

where

$$m\equiv m_0[A\pm(B^2+\tfrac{1}{6}C^2)^{1/2}]^{-1}\ . \tag{3}$$

Function $g$ is given, with a maximum error of approximately 0.9% for germanium, by

$$g=\eta\left[\left[\frac{k_x}{k}\right]^4+\left[\frac{k_y}{k}\right]^4+\left[\frac{k_z}{k}\right]^4-\frac{2}{3}\right]\ , \tag{4}$$

where

$$\eta\equiv\frac{\mp C^2}{4(B^2+\frac{1}{6}C^2)^{1/2}[A\pm(B^2+\frac{1}{6}C^2)^{1/2}]} \tag{5}$$

(see Ref. 2). The wave-vector dependence of $g$ reflects the warping and does cause cyclotron harmonic resonance. When an external magnetic field is applied, it is convenient to introduce a new set of coordinate axes by the following relations:

$$\begin{bmatrix}k_x\\k_y\\k_z\end{bmatrix}=\begin{bmatrix}t_{11}t_{12}t_{13}\\t_{21}t_{22}t_{23}\\t_{31}t_{32}t_{33}\end{bmatrix}\begin{bmatrix}k_1\\k_2\\k_3\end{bmatrix}\equiv T\begin{bmatrix}k_1\\k_2\\k_3\end{bmatrix}\ , \tag{6}$$

where $T$ is an orthogonal matrix, $k_3$ the wave-vector component parallel to the external magnetic field, and $k_1$ and $k_2$ two other perpendicular components. First, let us examine those holes whose wave numbers are such that $k_3^2\gg k_1^2+k_2^2$. Here $k_1^2+k_2^2$ is a good parameter to discuss cyclotron resonance, because the wave vector changes in a constant energy surface perpendicular to the external magnetic field. Substituting Eqs. (6) into Eq. (4) and expanding it in powers of $k_1/k_3$ and $k_2/k_3$, one obtains

$$g=\eta\left[\sum_m t_{m,3}^4\left[1+\frac{4\sum_n t_{n,3}^3t_{n,1}}{\sum_n t_{n,3}^4}\frac{k_1}{k_3}+\frac{4\sum_n t_{n,3}^3t_{n,2}}{\sum_n t_{n,3}^4}\frac{k_2}{k_3}+\cdots\right]-\frac{2}{3}\right]\ . \tag{7}$$

Using simple algebra and the property of the orthogonal matrix, one can easily show that $\sum_n t_{n,3}^3t_{n,1}$, etc. are of the order of unity at most and the following inequalities hold:

$$\tfrac{1}{3}\le\sum_m t_{m,3}^4\le 1\ . \tag{8}$$

If $k_1/k_3$ and $k_2/k_3$ are small enough compared to unity, then we have, in the zeroth-order approximation,

$$g\cong\eta\left[\sum_m t_{m,3}^4-\tfrac{2}{3}\right]\ , \tag{9}$$

thus $g$ becomes independent of wave vector. In this case the warping disappears and the transition probability of harmonic resonance vanishes. If such an assumption that $k_3^2\gg k_1^2+k_2^2$ is not applicable, then $g$ explicitly becomes a function of $k_1$, $k_2$, and $k_3$, that is, the warping effect remains and the transition probability of harmonic resonance exists except for special external magnetic-field directions.

The same conclusion can also be drawn from quantum theory. Then we see a clear distinction between fundamental and harmonic resonances in transition probability calculated from Luttinger's Hamiltonian. Details in the calculation of transition probabilities are described in the Appendix. The calculation with perturbation theory is applicable only when $\mathbf{B}\|[001]$. For such holes, whose

Landau quantum number $n$ is much smaller than $\zeta^2=\hbar k_3^2/eB$, the transition probabilities of fundamental cyclotron resonance as well as the third and the fifth harmonics are given by

$$\frac{1}{2}\frac{(\gamma_1\gamma_2\mp\gamma_2^2\pm 3\gamma_3^2)^2}{\gamma_2^2}(n+1)\,, \tag{10}$$

$$\frac{9}{8}\frac{(\gamma_2^2-\gamma_3^2)^2}{\gamma_2^2}(n+1)\frac{(n+2)(n+3)}{\zeta^4}\,, \tag{11}$$

and

$$\frac{225}{2048}\frac{(\gamma_2^2-\gamma_3^2)^2[\gamma_1(\gamma_2^2-3\gamma_3^2)\mp\gamma_2^3]^2}{\gamma_2^2(\gamma_1\gamma_2\mp\gamma_2^2\pm 3\gamma_3^2)^2}(n+1) \times\frac{(n+2)(n+3)(n+4)(n+5)}{\zeta^8} \tag{12}$$

multiplied by $2\pi\hbar^2e^3BE_2^2/m_0^2\omega^2$ for light holes (upper signs) and heavy holes (lower signs), respectively (see the Appendix). Here $\gamma_1$, $\gamma_2$, and $\gamma_3$ are Luttinger's band parameters[19] and $E_2$ the microwave electric field. The even-numbered harmonics are forbidden for $\mathbf{B}\|[001]$. One remarkable result is that the transition probability of fundamental resonance has no $\zeta$ dependence, while those of harmonics rapidly approach zero as $n/\zeta^2$ is decreased. This characteristic is the same as that obtained in the preceding consideration based on the wave-vector dependence of the warped energy surface. Landau quantum number $n$ and $\zeta$ in the quantum-mechanical treatment correspond to $k_1^2+k_2^2$ and $k_3$, respectively, appearing in the semiclassical treatment.

Let us next discuss the hot-hole distribution problem in terms of the above results. Figure 6 is a schematic energy diagram for the conduction, free-exciton, EHD, and valence bands in the presence of an external magnetic field. Only a single parabola is drawn, for simplicity, for the free-exciton or conduction band. We assume that hot holes populated in regions $A$ and $B$ have enough kinetic energy to break EHD. The transition probability of fundamental resonance has no $k_3$ dependence, so that hot holes produced by fundamental resonance can be distributed widely in the band; in other words, both in region $A$ and in region $B$. The transition probability of harmonics, on the other hand, rapidly approaches zero, as $n/\zeta^2$ or $(k_1^2+k_2^2)/k_3^2$ is decreased, so that harmonic resonance can hardly occur in region $B$. Hot holes produced by harmonic resonance, accordingly, tend to occupy region $A$. Only a limited number of holes are brought about in region $B$ through relaxation process of high-energy holes. It is thus concluded that hot holes produced by harmonic resonance mainly populate region $A$.

Finally we discuss the impact dissociation process of EHD by hot holes, referring to Fig. 6. The impact dissociation process occurs through the transition from a state below the Fermi energy in EHD to a free exciton state, and at the same time through the transition from a high-energy state of holes to a low-energy state, that is, the transition of an electron-hole pair from region $E$ or $F$ to region $G$ or $H$, and the transition of a hole from region $A$ or $B$ to region $C$. The density of states of energy bands in

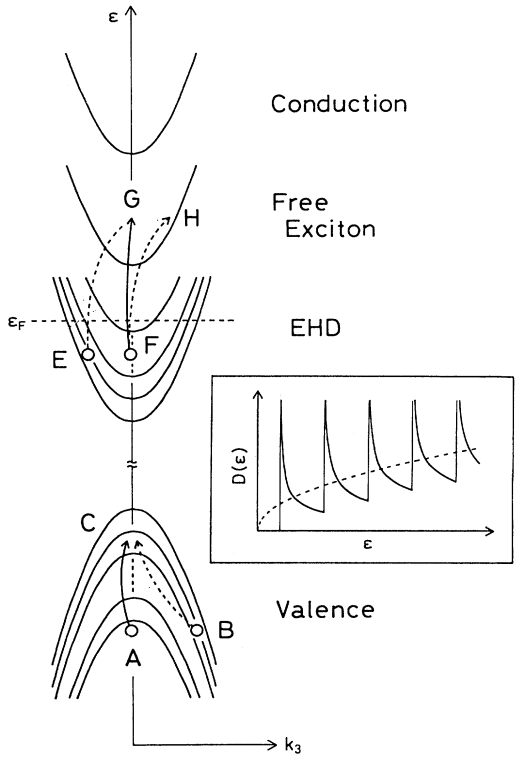


FIG. 6. Schematic energy diagram of the conduction, free-exciton, EHD, and valence bands in the presence of a magnetic field. Only a single parabola is drawn to express the free-exciton or conduction band for simplicity. The light-hole band is also abbreviated. The states of free excitons and EHD may be regarded as those of electron-hole pairs. A pair of solid arrows indicates dominant process in the impact dissociation phenomenon of EHD by hot holes. The inset shows schematic density of states of energy bands under the magnetic field.

the presence of a magnetic field is characterized by the one-dimensional scheme. At any energy level, the density of states mainly consists of the states such that $k_3\approx 0$ (see the inset in Fig. 6). Here note that this situation holds even under no magnetic field. The reason is as follows: Assuming isotropic effective mass $m^*$, one can write the density of states $D(E)$ by

$$D(\varepsilon)\delta\varepsilon\propto\sum_{\varepsilon=\text{const}}\delta k_1\delta k_2\delta k_3\,, \tag{13}$$

where

$$\varepsilon=\frac{\hbar^2}{2m^*}(k_1^2+k_2^2+k_3^2)\,. \tag{14}$$

If we introduce cylindrical coordinates, Eq. (13) is rewritten as

$$D(\varepsilon)\delta\varepsilon\propto\sum_{\varepsilon=\text{const}}\sqrt{2m^*\varepsilon/\hbar^2-k_3^2}\,\delta\rho\delta k_3\,, \tag{15}$$

where

$$\rho=(k_1^2+k_2^2)^{1/2}\,. \tag{16}$$

Each term on the right-hand side is largest when $k_3=0$. Thus at any energy level, the density of states mainly consists of the states such that $k_3\approx 0$. Though the free exciton or EHD states in the presence of a magnetic field are generally complicated, the same situation as above will still hold. In Fig. 6, regions $A$, $C$, $F$, and $G$ consist of a number of states. The dominant process will be the transition between the regions with accumulated density of states. For an electron-hole pair in EHD, the transition from region $F$ to region $G$ should be dominant in the impact dissociation process. It is hot holes in region $A$ that can contribute to this process to satisfy the law of momentum conservation. If hot holes in region $B$ drive electron-hole pairs in region $F$ to region $G$, the process needs to include phonon absorption or emission to conserve momentum. That is a transition of higher order. As a result, the transition probability of this process is small. It is true that hot holes in region $B$ can also drive electron-hole pairs from region $E$ to region $G$ as well as from region $F$ to region $H$ without phonon absorption or emission. But regions $E$ and $H$ consist of only a small number of states. Consequently, the transition rates of these processes must be small.

From the above discussion, we expect that hot holes in region $A$ are efficient for breaking EHD, while those in region $B$ are not. Hot holes produced by harmonic resonance mainly populate region $A$, so that they break EHD more efficiently than those produced by fundamental resonance, which populate region $B$ as well as region $A$. For this reason, we can conclude that the relative intensity of harmonic against fundamental resonance is larger in ODCR than in CR.

## V. SUMMARY AND CONCLUSIONS

We have investigated ODCR and CR under the completely identical condition. There exist two remarkable characteristics; namely, (1) strength of the hole cyclotron resonance compared with that of the electron resonance is more pronounced in ODCR than in CR, and (2) relative strength of the cyclotron harmonic resonance to the fundamental is larger in ODCR than in CR. Owing to these two advantages, the ODCR technique is considered to be exceedingly successful in observing characteristic behavior of hole cyclotron resonance and its harmonics; and we have clearly observed harmonic resonances to third order for light holes and to sixth order for heavy holes by means of ODCR.

By considering the wave-vector dependence of warped hole bands and the transition probabilities of cyclotron resonance as well as its harmonics, we have proved that hot holes produced by cyclotron fundamental resonance are distributed rather uniformly in the wave-vector space, while those produced by harmonic resonance are localized in region $A$ in Fig. 6. On the basis of this situation, we have explained the reason why harmonic resonance is pronounced in ODCR. Peculiar signals of harmonics in ODCR reflect one-sided distribution in the wave-vector space of hot holes produced by harmonic resonance.

## ACKNOWLEDGMENTS

The authors thank H. Nakata and K. Fujii for their suggestion and useful help. This work was partially supported by a Grant-in-Aid for Scientific Research on Priority Areas from the Ministry of Education, Science, and Culture. One of the authors (T.T.) has been supported by the Japan Society for the Promotion of Science.

## APPENDIX

We will calculate the transition probabilities of hole cyclotron resonance and its harmonics for $\mathbf{B}\|[001]$ by means of perturbation theory using Luttinger's Hamiltonian.[19] We choose units such that $\hbar=1$ for simplicity, and later restore $\hbar$. Luttinger's Hamiltonian is given by

$$D=\frac{1}{m_0}[(\gamma_1+\tfrac{5}{2}\gamma_2)\frac{k^2}{2}-\gamma_2(k_x^2J_x^2+k_y^2J_y^2+k_z^2J_z^2)$$
$$-2\gamma_3(\{k_x,k_y\}\{J_x,J_y\}+\{k_y,k_z\}\{J_y,J_z\}+\{k_z,k_x\}\{J_z,J_x\})+e\kappa\mathbf{J}\cdot\mathbf{B}+eq(J_x^3B_x+J_y^3B_y+J_z^3B_z)]\ , \tag{A1}$$

where

$$\{k_x,k_y\}=\tfrac{1}{2}(k_xk_y+k_yk_x),\quad \text{etc.}\ , \tag{A2}$$

$$\mathbf{k}=\mathbf{p}+e\,\mathbf{A}\ . \tag{A3}$$

Here $\gamma_1$, $\gamma_2$, $\gamma_3$, $\kappa$, and $q$ are Luttinger's band parameters, $\mathbf{p}$ the momentum operator, and $\mathbf{A}$ the vector potential. The operators $\mathbf{J}$ satisfy commutation relations of spin $\frac{3}{2}$. The subscripts $x$, $y$, and $z$ indicate the crystal principal axes. We confine ourselves to the magnetic field in the $(\bar{1}10)$ plane. If we call $\theta$ the angle between the field and the $z$ axis, then we can choose such a new (1,2,3) coordinate system that

$$k_x=\frac{1}{\sqrt{2}}(ck_1-k_2+sk_3)\ ,$$
$$k_y=\frac{1}{\sqrt{2}}(ck_1+k_2+sk_3)\ , \tag{A4}$$
$$k_z=-sk_1+ck_3\ ,$$

where $s\equiv\sin\theta$ and $c\equiv\cos\theta$. The 2 axis and 3 axis are parallel to the $[\bar{1}10]$ direction and to the magnetic field, respectively. The relation between $J_x,J_y,J_z$ and $J_1,J_2,J_3$ is also given by (A4). We define

$$k_1 \equiv \sqrt{eB}\,\frac{a+a^+}{\sqrt{2}}\ ,$$
$$k_2 \equiv \sqrt{eB}\,i\frac{a-a^+}{\sqrt{2}}\ , \qquad \text{(A5)}$$
$$k_3 \equiv \sqrt{eB}\,\zeta\ ,$$

where $[a,a^+]=1$ because of $[k_1,k_2]=eB/i$. Now we confine ourselves to $\mathbf{B}\|[001]$, leading to $c=1$ and $s=0$. Since $q$ is very small,[4] we use an approximation of $q=0$. Then (A1) is rewritten as

$$\begin{aligned} D=\frac{eB}{m_0}\Bigg[&(\gamma_1+\tfrac{5}{2}\gamma_2)\left(a^+a+\frac{1}{2}+\frac{\zeta^2}{2}\right)\\ &-\gamma_2[(a^+a+\tfrac{1}{2})(J_1^2+J_2^2)+\zeta^2J_3^2\\ &\quad+i(a^2-a^{+2})\{J_1,J_2\}]\\ &-\gamma_3\Bigg[\frac{a^2+a^{+2}}{2}(J_1^2-J_2^2)+i\sqrt{2}(a-a^+)\zeta\{J_2,J_3\}\\ &\quad+\sqrt{2}(a+a^+)\zeta\{J_3,J_1\}\Bigg]+\kappa J_3\Bigg]\ . \end{aligned} \qquad \text{(A6)}$$

Here we chose the following representations for $J_1$, $J_2$, and $J_3$:

$$J_1=\begin{Vmatrix} 0 & \frac{\sqrt{3}}{2} & 0 & 0\\ \frac{\sqrt{3}}{2} & 0 & 1 & 0\\ 0 & 1 & 0 & \frac{\sqrt{3}}{2}\\ 0 & 0 & \frac{\sqrt{3}}{2} & 0 \end{Vmatrix},$$

$$J_2=\begin{Vmatrix} 0 & -\frac{\sqrt{3}}{2}i & 0 & 0\\ \frac{\sqrt{3}}{2}i & 0 & -i & 0\\ 0 & i & 0 & -\frac{\sqrt{3}}{2}i\\ 0 & 0 & \frac{\sqrt{3}}{2}i & 0 \end{Vmatrix}, \qquad \text{(A7)}$$

$$J_3=\begin{Vmatrix} \frac{3}{2} & 0 & 0 & 0\\ 0 & \frac{1}{2} & 0 & 0\\ 0 & 0 & -\frac{1}{2} & 0\\ 0 & 0 & 0 & -\frac{3}{2} \end{Vmatrix}.$$

The choice of these representations is slightly different from that in Ref. 19. Now we get a concrete representation of (A6), i.e.,

$$D=D_0+D_1\ ,$$

with

$$D_0=\frac{eB}{m_0}\begin{Vmatrix} (\gamma_1+\gamma_2)(N+\frac{1}{2})+(\gamma_1-2\gamma_2)\frac{\zeta^2}{2}+\frac{3}{2}\kappa & -\sqrt{6}\gamma_3 a\zeta & 0 & 0\\ -\sqrt{6}\gamma_3 a^+\zeta & (\gamma_1-\gamma_2)(N+\frac{1}{2})+(\gamma_1+2\gamma_2)\frac{\zeta^2}{2}+\frac{1}{2}\kappa & 0 & 0\\ 0 & 0 & (\gamma_1-\gamma_2)(N+\frac{1}{2})+(\gamma_1+2\gamma_2)\frac{\zeta^2}{2}-\frac{1}{2}\kappa & \sqrt{6}\gamma_3 a\zeta\\ 0 & 0 & \sqrt{6}\gamma_3 a^+\zeta & (\gamma_1+\gamma_2)(N+\frac{1}{2})+(\gamma_1-2\gamma_2)\frac{\zeta^2}{2}-\frac{3}{2}\kappa \end{Vmatrix} \qquad \text{(A8)}$$

and

$$D_1=\frac{eB}{m_0}\begin{Vmatrix} 0 & -\frac{\sqrt{3}}{2}(\gamma_2+\gamma_3)a^2+\frac{\sqrt{3}}{2}(\gamma_2-\gamma_3)a^{+2} & 0 & 0\\ -\frac{\sqrt{3}}{2}(\gamma_2+\gamma_3)a^{+2}+\frac{\sqrt{3}}{2}(\gamma_2-\gamma_3)a^2 & 0 & 0 & 0\\ 0 & 0 & 0 & -\frac{\sqrt{3}}{2}(\gamma_2+\gamma_3)a^{+2}+\frac{\sqrt{3}}{2}(\gamma_2-\gamma_3)a^2\\ 0 & 0 & -\frac{\sqrt{3}}{2}(\gamma_2+\gamma_3)a^2+\frac{\sqrt{3}}{2}(\gamma_2-\gamma_3)a^{+2} & 0 \end{Vmatrix}. \qquad \text{(A9)}$$

Here $N=a^{+}a$. From now on, we consider the case of $\zeta^2$, $\zeta^2/n \gg 1$. We solve the eigenvalue problem by regarding $D_1$ as a perturbation. Since the zeroth-order Hamiltonian $D_0$ breaks up into two $2\times 2$ matrix operators, we can easily obtain eigenvalues $\varepsilon^0$ and eigenvectors $\psi^0$:

$$\varepsilon^0_{1,n}=\frac{eB}{m_0}\left[(\gamma_1-2\gamma_2)\frac{\zeta^2}{2}+\left[\gamma_1+\gamma_2-3\frac{\gamma_3^2}{\gamma_2}\right]n+\frac{1}{2}\left[\gamma_1+\gamma_2-6\frac{\gamma_3^2}{\gamma_2}+3\kappa\right]\right.$$
$$\left.-\frac{3}{2}\frac{\gamma_3^2}{\gamma_2}\frac{n+1}{\zeta^2}\left[2(n+1)-\frac{\gamma_1}{\gamma_2}+\frac{\kappa}{\gamma_2}-3\frac{\gamma_3^2}{\gamma_2^2}(n+1)\right]+O\left[\frac{1}{\zeta^4}\right]\right], \tag{A10}$$

$$\psi^0_{1,n}=\left|\left|\begin{matrix}c_1u_n\\ c_2u_{n+1}\end{matrix}\right|\right|=\left|\left|\begin{matrix}\left[1-\frac{3}{4}\frac{\gamma_3^2}{\gamma_2^2}\frac{(n+1)}{\zeta^2}+O\left[\frac{1}{\zeta^4}\right]\right]u_n\\ \frac{\sqrt{6}}{2}\frac{\gamma_3}{\gamma_2}\frac{\sqrt{n+1}}{\zeta}\left[1-\frac{9}{4}\frac{\gamma_3^2}{\gamma_2^2}\frac{n+1}{\zeta^2}+\frac{n+1}{\zeta^2}-(\gamma_1-\kappa)\frac{1}{2\gamma_2\zeta^2}+O\left[\frac{1}{\zeta^4}\right]\right]u_{n+1}\end{matrix}\right|\right|, \tag{A11}$$

and

$$\varepsilon^0_{2,n}=\frac{eB}{m_0}\left[(\gamma_1+2\gamma_2)\frac{\zeta^2}{2}+\left[\gamma_1-\gamma_2+3\frac{\gamma_3^2}{\gamma_2}\right]n+\tfrac{1}{2}(\gamma_1-\gamma_2+\kappa)+\frac{3}{2}\frac{\gamma_3^2}{\gamma_2}\frac{n}{\zeta^2}\left[2n-\frac{\gamma_1}{\gamma_2}+\frac{\kappa}{\gamma_2}-3\frac{\gamma_3^2}{\gamma_2^2}n\right]+O\left[\frac{1}{\zeta^4}\right]\right], \tag{A12}$$

$$\psi^0_{2,n}=\left|\left|\begin{matrix}c_1'u_{n-1}\\ c_2'u_n\end{matrix}\right|\right|=\left|\left|\begin{matrix}-\frac{\sqrt{6}}{2}\frac{\gamma_3}{\gamma_2}\frac{\sqrt{n}}{\zeta}\left[1-\frac{9}{4}\frac{\gamma_3^2}{\gamma_2^2}\frac{n}{\zeta^2}+\frac{n}{\zeta^2}-(\gamma_1-\kappa)\frac{1}{2\gamma_2\zeta^2}+O\left[\frac{1}{\zeta^4}\right]\right]u_{n-1}\\ \left[1-\frac{3}{4}\frac{\gamma_3^2}{\gamma_2^2}\frac{n}{\zeta^2}+O\left[\frac{1}{\zeta^4}\right]\right]u_n\end{matrix}\right|\right| \tag{A13}$$

from the upper $2\times 2$ block, and similarly

$$\varepsilon^0_{3,n}=\frac{eB}{m_0}\left[(\gamma_1+2\gamma_2)\frac{\zeta^2}{2}+\left[\gamma_1-\gamma_2+3\frac{\gamma_3^2}{\gamma_2}\right]n+\frac{1}{2}\left[\gamma_1-\gamma_2+6\frac{\gamma_3^2}{\gamma_2}-\kappa\right]\right.$$
$$\left.-\frac{3}{2}\frac{\gamma_3^2}{\gamma_2}\frac{n+1}{\zeta^2}\left[-2(n+1)-\frac{\gamma_1}{\gamma_2}+\frac{\kappa}{\gamma_2}+3\frac{\gamma_3^2}{\gamma_2^2}(n+1)\right]+O\left[\frac{1}{\zeta^4}\right]\right], \tag{A14}$$

$$\psi^0_{3,n}=\left|\left|\begin{matrix}c_3'u_n\\ c_4'u_{n+1}\end{matrix}\right|\right|=\left|\left|\begin{matrix}\left[1-\frac{3}{4}\frac{\gamma_3^2}{\gamma_2^2}\frac{n+1}{\zeta^2}+O\left[\frac{1}{\zeta^4}\right]\right]u_n\\ \frac{\sqrt{6}}{2}\frac{\gamma_3}{\gamma_2}\frac{\sqrt{n+1}}{\zeta}\left[1-\frac{9}{4}\frac{\gamma_3^2}{\gamma_2^2}\frac{n+1}{\zeta^2}+\frac{n+1}{\zeta^2}+(\gamma_1-\kappa)\frac{1}{2\gamma_2\zeta^2}+O\left[\frac{1}{\zeta^4}\right]\right]u_{n+1}\end{matrix}\right|\right|, \tag{A15}$$

and

$$\varepsilon^0_{4,n}=\frac{eB}{m_0}\left[(\gamma_1-2\gamma_2)\frac{\zeta^2}{2}+\left[\gamma_1+\gamma_2-3\frac{\gamma_3^2}{\gamma_2}\right]n+\tfrac{1}{2}(\gamma_1+\gamma_2-3\kappa)\right.$$
$$\left.+\frac{3}{2}\frac{\gamma_3^2}{\gamma_2}\frac{n}{\zeta^2}\left[-2n-\frac{\gamma_1}{\gamma_2}+\frac{\kappa}{\gamma_2}+3\frac{\gamma_3^2}{\gamma_2^2}n\right]+O\left[\frac{1}{\zeta^4}\right]\right], \tag{A16}$$

$$\psi^0_{4,n}=\left|\left|\begin{matrix}c_3u_{n-1}\\ c_4u_n\end{matrix}\right|\right|=\left|\left|\begin{matrix}-\frac{\sqrt{6}}{2}\frac{\gamma_3}{\gamma_2}\frac{\sqrt{n}}{\zeta}\left[1-\frac{9}{4}\frac{\gamma_3^2}{\gamma_2^2}\frac{n}{\zeta^2}+\frac{n}{\zeta^2}+(\gamma_1-\kappa)\frac{1}{2\gamma_2\zeta^2}+O\left[\frac{1}{\zeta^4}\right]\right]u_{n-1}\\ \left[1-\frac{3}{4}\frac{\gamma_3^2}{\gamma_2^2}\frac{n}{\zeta^2}+O\left[\frac{1}{\zeta^4}\right]\right]u_n\end{matrix}\right|\right| \tag{A17}$$

from the lower $2\times 2$ block, where $n=0,1,2,\ldots$ and $u_n$ is the eigenfunction of the harmonic oscillator. The function $u_{-1}$ has no significance. The second-order eigenvector is given by the formula of perturbation theory:

$$\psi_{\alpha,n}=\psi^0_{\alpha,n}+\sum_{i,l}{}'\psi^0_{i,l}\frac{(\psi^0_{i,l},D_1\psi^0_{\alpha,n})}{\varepsilon^0_{\alpha,n}-\varepsilon^0_{i,l}}+\sum_{i,l}{}'\sum_{j,m}{}'\psi^0_{i,l}\frac{(\psi^0_{i,l},D_1\psi^0_{j,m})(\psi^0_{j,m},D_1\psi^0_{\alpha,n})}{(\varepsilon^0_{\alpha,n}-\varepsilon^0_{i,l})(\varepsilon^0_{\alpha,n}-\varepsilon^0_{j,m})}$$
$$+\sum_{i,l}{}'\psi^0_{i,l}\frac{(\psi^0_{\alpha,n},D_1\psi^0_{\alpha,n})(\psi^0_{i,l},D_1\psi^0_{\alpha,n})}{(\varepsilon^0_{\alpha,n}-\varepsilon^0_{i,l})^2}\ . \tag{A18}$$

Here $\alpha=1,4$ and $\alpha=2,3$ correspond to heavy- and light-hole types, respectively.

The perturbation giving electric dipole transitions induced by the microwave electric field $\mathbf{E}=E_2\hat{\mathbf{e}}_2$, where $\hat{\mathbf{e}}_2$ is a unit vector of the 2 axis, is given by introducing a vector potential

$$\mathbf{A}'=(i/\omega)\mathbf{E}\ . \tag{A19}$$

The perturbation matrix $D_2$ is obtained by replacing $\mathbf{k}$ in (A3) by $\mathbf{k}+e\,\mathbf{A}'$, and retaining terms of first order in $\mathbf{E}$. The result is

$$D_2=\frac{eE_2}{\omega_0\omega}\sqrt{eB}\begin{Vmatrix} -\frac{1}{\sqrt{2}}(\gamma_1+\gamma_2)(a-a^+) & -\sqrt{3}\gamma_3\xi & -\sqrt{3/2}(\gamma_2+\gamma_3)a & 0 \\ & & -\sqrt{3/2}(\gamma_2-\gamma_3)a^+ & \\ \sqrt{3}\gamma_3\xi & -\frac{1}{\sqrt{2}}(\gamma_1-\gamma_2)(a-a^+) & 0 & -\sqrt{3/2}(\gamma_2+\gamma_3)a \\ & & & -\sqrt{3/2}(\gamma_2-\gamma_3)a^+ \\ \sqrt{3/2}(\gamma_2+\gamma_3)a^+ & 0 & -\frac{1}{\sqrt{2}}(\gamma_1-\gamma_2)(a-a^+) & \sqrt{3}\gamma_3\xi \\ +\sqrt{3/2}(\gamma_2-\gamma_3)a & & & \\ 0 & \sqrt{3/2}(\gamma_2+\gamma_3)a^+ & -\sqrt{3}\gamma_3\xi & -\frac{1}{\sqrt{2}}(\gamma_1+\gamma_2)(a-a^+) \\ & +\sqrt{3/2}(\gamma_2-\gamma_3)a & & \end{Vmatrix}\ . \tag{A20}$$

If we revive $\hbar$, the transition probability is given by

$$\frac{2\pi}{\hbar}|(\psi_{\alpha,m},D_2\psi_{\alpha,n})|^2\ . \tag{A21}$$

The cases of $\alpha=1$ and $\alpha=4$ lead to the same results, and similarly for the cases of $\alpha=2$ and $\alpha=3$. If we retain terms of the lowest order in $(1/\xi)$ in the final results, the transition probabilities of fundamental resonance, the third harmonic, and the fifth are given by

$$\frac{1}{2}\frac{(\gamma_1\gamma_2\mp\gamma_2^2\pm3\gamma_3^2)^2}{\gamma_2^2}(n+1)\ ,$$
$$\frac{9}{8}\frac{(\gamma_2^2-\gamma_3^2)^2}{\gamma_2^2}(n+1)\frac{(n+2)(n+3)}{\xi^4}\ , \tag{A22}$$
$$\frac{225}{2048}\frac{(\gamma_2^2-\gamma_3^2)^2[\gamma_1(\gamma_2^2-3\gamma_3^2)\mp\gamma_2^3]^2}{\gamma_2^2(\gamma_1\gamma_2\mp\gamma_2^2\pm3\gamma_3^2)^2}(n+1)\frac{(n+2)(n+3)(n+4)(n+5)}{\xi^8}$$

multiplied by $2\pi\hbar^2e^3BE_2^2/m_0^2\omega^2$, respectively. Here the upper signs are for light holes and the lower signs for heavy holes. The transition probability of the third harmonic is identical for both light and heavy holes. The even-numbered harmonics are forbidden.

[1]R. N. Dexter, H. J. Zeiger, and B. Lax, Phys. Rev. **104**, 637 (1956).
[2]H. J. Zeiger, B. Lax, and R.N. Dexter, Phys. Rev. **105**, 495 (1957).
[3]K. Suzuki and J. C. Hensel, Phys. Rev. B **9**, 4184 (1974).
[4]J. C. Hensel and K. Suzuki, Phys. Rev. B **9**, 4219 (1974).
[5]R. F. Wallis and H. J. Bowlden, Phys. Rev. **118**, 456 (1961).
[6]See, for example, A. Andronov, in *Proceedings of the 19th International Conference on the Physics of Semiconductors, Warsaw, 1988,* edited by W. Zawadzki (Institute of Physics, Polish

Academy of Sciences, 1988), p. 1383.
[7]See, for example, E. Otsuka, Jpn. J. Appl. Phys. **25**, 303 (1986).
[8]G. Dresselhaus, A. F. Kip, and C. Kittel, Phys. Rev. **98**, 368 (1955).
[9]I. G. Gverdtsiteli, L. N. Aleksandrov, and L. V. Ovchinnikova, Fiz. Tverd. Tela (Leningrad) **11**, 572 (1969) [Sov. Phys. Solid State **11**, 463 (1969)].
[10]P. G. Baranov, Yu. P. Veshchunov, R. A. Zhitnikov, N. G. Romanov, and Yu. G. Shreter, Pis'ma Zh. Eksp. Teor. **26**, 369 (1977) [JETP Lett. **26**, 249 (1977)].
[11]R. Romestain and C. Weisbuch, Phys. Rev. Lett. **45**, 2067 (1980).
[12]Le Si Dang, G. Neu, and R. Romestain, Solid State Commun. **44**, 1187 (1982).
[13]I. J. Booth and C. F. Schwerdtfeger, Phys. Status Solidi B **130**, 749 (1985).
[14]I. J. Booth and C. F. Schwerdtfeger, Solid State Commun. **55**, 817 (1985).
[15]B. C. Cavenett and E. J. Pakulis, Phys. Rev. B **32**, 8449 (1985).
[16]E. J. Pakulis and G. A. Northrop, Appl. Phys. Lett. **50**, 1672 (1987).
[17]T. Tomaru, T. Ohyama, and E. Otsuka, J. Phys. Soc. Jpn. **58**, 3718 (1989).
[18]J. M. Luttinger and W. Kohn, Phys. Rev. **97**, 869 (1955).
[19]J. M. Luttinger, Phys. Rev. **102**, 1030 (1956).
[20]See reviews by T. M. Rice and J. C. Hensel, T. G. Phillips, and G. A. Thomas, in *Solid State Physics,* edited by H. Ehrenreich, F. Seitz, and D. Turnbull (Academic, New York, 1977), Vol. 32.
[21]B. W. Levinger and D. R. Frankl, J. Phys. Chem. Solids **20**, 281 (1961).
[22]J. J. Stickler, H. J. Zeiger, and G. S. Heller, Phys. Rev. **127**, 1077 (1962).
[23]T. Tomaru, T. Ohyama, and E. Otsuka, in *Proceedings of the 20th International Conference on the Physics of Semiconductors, Thessaloniki, 1990,* edited by E. M. Anastassakis and J. D. Joannopoulos (World Scientific, Singapore, 1990), p. 630.